Structural, optical and mechanical properties of cobalt copper oxides coatings synthesized from low concentrations of sol-gel process

Amun Amri[1,*], Zhong-Tao Jiang[2], Chun-Yang Yin[3], Ahmad Fadli[1], M. Mahbubur Rahman[2], Syaiful Bahri[1], Hantarto Widjaja[2], Nicholas Mondinos[2], Tutut Herawan[4], M. Miftahul Munir[5], Gadang Priyotomo[6]

[1] Department of Chemical Engineering, Universitas Riau, Kampus UR Panam, Pekanbaru, Riau 28293, Indonesia
[2] School of Engineering & Information Technology, Murdoch University, 6150 WA, Australia
[3] School of Science & Engineering, Teesside University, Middlesbrough, United Kingdom
[4] Universitas Teknologi Yogyakarta, and AMCS Research Center, Yogyakarta, Indonesia
[5] Department of Physics, Institut Teknologi Bandung (ITB), Bandung, Indonesia
[6] Indonesian Institute of Sciences (LIPI), Serpong, Tangerang, Indonesia

Received ...., revised ...., accepted ....
Published online .....

Keywords Cobalt copper oxides, low concentration sol-gel coating, structural, absorptance, nanoindentation.

*Corresponding author: amun.amri@eng.unri.ac.id , Phone: +62 823 8176 0767, Fax: +62 761 566 937

Abstract. Thin films of $Co_xCu_yO_z$ have been coated on aluminium substrates via sol-gel route using low concentration of copper and cobalt precursors at annealing temperatures in range of 500°C - 650°C. The coatings were characterized by X-ray diffraction (XRD), X-ray photoelectron spectroscopy (XPS), UV-Vis-NIR spectrophotometry and nanoindentation. The XRD analysis in 2θ-range of 30°-42° revealed that the coatings exhibited low crystallinity of $CoCu_2O_3$, $CoCuO_2$ and $CuCoO_2$. The surface bonding structure analyzed using XPS indicated that the coating contained: Cu (tetrahedral Cu^+ and octahedral Cu^{2+}), Co (octahedral Co^{3+} , tetrahedral Co^{2+} and mixed Co^{2+} and Co^{3+}), and O (lattice, surface and sub-surface oxygens). The optical properties characterized using UV-Vis-NIR showed that the reflectance spectra of coatings formed a spectrally solar selective absorber profile associated with the interference peaks and the absorption edges around wavelengths of below 1.2 µm. The maximum absorptance (α =75.8%) was shown by coating synthesized at 500 °C. The mechanical properties of coatings showed that the increase of anealling temperature increased the coating's hardness (*H*) and the elastic modulus (*E*) due to the enhancement of the $[CoCuO_2/CuCoO_2]$:$[CoCu_2O_3]$ oxide phases ratio, as the result, an excellent stability of the wear resistance (*H*/*E*) of around ~0.035 was recorded.

1 Introduction Cobalt and copper mixed oxides have found widespread applications such as catalyst for many important reactions (*e.g.* oxygen evolution reactions (OER), the Fischer−Tropsch process, *etc*.) and as thermoelectric materials [1-4]. The physicochemical, electrochemical, magnetic, conductivity and thermal properties have been substantially studied by various researches [5-8]. A major conclusion reached is that the chemical nature and the compositions of the precursors, as well as the annealing treatments influence the properties of these mixed oxides *i.e* properties are influenced by the preparation method [1, 3, 5, 9, 10]. The term "Co and Cu mixed oxides" will be denoted by CoO/CuO for short in the rest of the manuscript.

The surface chemical activity and selectivity of the CoO/CuO are markedly affected by the precursors composition that provide a high surface area as well as small and fairly uniform particle sizes which enhance the production of a well interdispersed CoO/CuO state. Further, the interdispersed state in the mixed oxides system

may interact giving rise to synergetic effects [10]. In the case of the spinel-type of CoO/CuO, the precursor ratio and the annealing temperatures influence the formation of the major crystall structure and separate minor phases composed of new cobalt and/or copper oxides [1, 9]. Normally the degree of crystallinity of the phases in CoO/CuO increases with rising annealing temperature. However a decrease in the degree of crystallinity is observed in phases synthesized from low copper precursor concentration [8].

Apart from the previous mentioned properties, the optical and mechanical properties of cobalt-copper mixed oxides coatings are comparatively less studied. In our previous work we studied the physico-chemical properties of cobalt-based mixed metal oxide ($M_xCo_yO_z$ with M=Mn, Cu, Ni) and $Co_xCu_yO_z$-SiO_2 coatings on Al substrate synthesized via sol-gel method at anealling temperature of 500°C. The optical properties of the coatings exhibited distinctive spectral selectivity in the solar wavelengths region (<2.5 µm) making them promising material for solar selective absorber (SSA) aplications [4,7]. In present work we synthesize $Co_xCu_yO_z$ thin film coatings via sol-gel process using low concentration of [Cu] and [Co] sol precursor (<0.2M). We investigate the effects of various annealing temperatures on the structural, surface electronic compositions, optical and mechanical properties (wear resistance) of the coatings. The synthesis conditions were optimised to obtain an improvement of mechanical stability and reproducibility of SSA optical coatings. Throughout the studies we found that the coatings synthesized using a low concentration of sol precursors (thereby enhancing cost-effectiveness of the coatings) underwent the increase of the [$CoCuO_2$/$CuCoO_2$]:[$CoCu_2O_3$] oxide phases ratio as the annealing temperature was increased, and this has a positive impact to retaining the wear resistance (hardness (*H*) per elastic modulus (*E*), *H*/*E*) of coating from the degradations.

2 Material and methods

2.1 Samples preparation A series of cobalt copper oxide thin film coatings tandem on Al substrates was synthesized *via* simple sol-gel dip-coating route as follows. Cobalt chloride and copper acetate were mixed in absolute ethanol, with the addition of propionic acid to form cobalt chloride (0.15 M) and copper acetate (0.15 M) mixed solutions. The mixed solutions was then stirred for 2 hours before being deposited on the clean aluminium substrates using a dip-coater at withdrawal rate of 120 mm/min and subsequently dryed on a hot plate at 150°C for 10 seconds. The optimized four times dip-drying cycles were carried out before final atmospheric annealing at temperatures ranging from 500 °C to 650 °C for 1 hour. The maximum heat treatment was limited due to the significant decrease of mechanical strengths on aluminum substrat at temperature above 670 °C.

2.2 Characterizations Minerlogical properties of the thin films coatings were characterized using a Bruker Advance D8 X-Ray Diffractometer (XRD) equipped with a Lynx-Eye detector Cu-tube and operated at 40kV/ 40mA [11, 12]. The X-ray photoelectron spectroscopy (XPS) (Kratos Axis Ultra XPS spectrometer, Manchester, UK) with Al Kα radiation ($h\nu$ = 1486.6 eV) was used to probe the surface compositions and chemical bonding structures of coatings. For quantification analysis, the CASA XPS (V.2.3.15) software was utilized using Shirley background subtraction. Jasco V-670 double beam UV–Vis-NIR spectrophotometer with integrating sphere was used to obtain the reflectance spectra of samples in wavelengths range of 0.3 to 2.7 µm. The solar absorptance value was calculated based on the AM1.5 standard as described in Duffie-Beckman [13].

The mechanical properties of film coatings were characterized using nano-indentation workstation (Ultra-Micro Indentation System 2000, CSIRO, Sydney, Australia) equipped with a Berkovich indenter. Nano-indentation test was conducted under load control with a maximum load of 0.5mN, under which the maximum penetration depth was found to be less than 10% of the film thickness. It was carried out to ensure that only the film properties were measured. For each test, 10 incremental and 10 decremental steps were used. For each sample, 30 measurements were taken, and then the results were averaged and the standard deviation was evaluated.

3 Results and discussion

3.1. Structural analysis Figure 1 shows the XRD patterns of the samples synthesized at different annealing temperatures. The overall XRD spectra are shown in Figure 1a. The peaks at *ca* 45° are from the Al substrate [from comparison to XRD spectra of the substrate]. Figure 1b shows the spectra in the range 30° – 42°with a magnified scale of the intensity. The peaks in this range are due to the mixed oxides coating clearly indicating the crystallinity of observed phases.

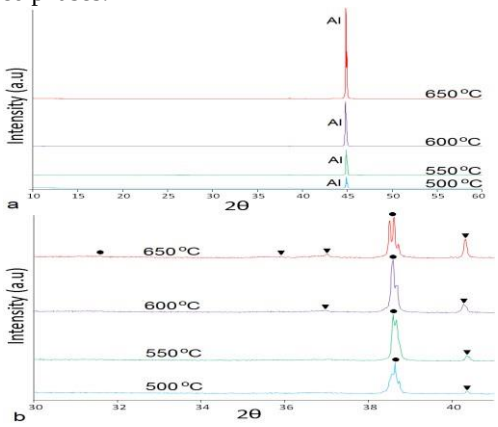

Figure 1. (a). XRD patterns of the cobalt-copper coatings deposited on aluminium substrate at different annealing temperatures, (b). Expanded XRD patterns within the region of 30-42°

Based on the peak's positions, intensities, *d*-spacing and ICDD databases, peaks at 35.9° (011), 36.9° (310) and 40.3° (301) (denoted "▼") are due to $CoCu_2O_3$ (ICDD 76-0442) (Fig. 1b). The intensity and crystallinity of the (301) direction increases extensively as the annealing temperature is increased from 500 °C to 650 °C suggesting a preferred orientation and increased domain size in this direction. The peaks at the approximately 38° - 39° range and 31.3° range are assigned to mixed phases of $CoCuO_2$ and $CuCoO_2$ (denoted "•") (ICDD 74-1855 and 21-0256 respectively).

Table 1 Crystal structures for some cobalt copper oxides

Crystal	No. of atoms in a unit cell	Space group	*a* (Å)	*b* (Å)	*c* (Å)	α (°)	*Z*
$CoCu_2O_3$	Co=2, Cu=4, O=6	Pmmn (59)	9.41^ 9.27* 9.62#	3.98^ 3.94* 4.05#	3.20^ 3.24* 2.99#		2
$CoCuO_2$ or $CuCoO_2$	Co=1, Cu=1, O=2	R-3m (166)	5.95~ 5.95* 5.88†			27.7~ 27.14* 28.07†	1

^ XRD database ICDD 76-0442; ~ XRD (ICDD 74- 1855);
† simulated using VASP, with *k*-points 5 × 5 × 5;
* calculated from our XRD experiment data;
# simulated using VASP, with *k*-points 4 × 8 × 10.

The percentage proportion of the 3 main oxide phases can be approximated from the intensity and width profiles of the $CoCu_2O_3$ and $CoCuO_2$ / $CuCoO_2$ peaks. At the highest annealing temperature of 650°C we approximate a [$CoCuO_2$ / $CuCoO_2$] : [$CoCu_2O_3$] oxide phases ratio of 3:2. A similar analysis of our previous work using higher [Co] and [Cu] sol precursors (0.25 M for each) showed a [$CoCuO_2$/$CuCoO_2$]:[$CoCu_2O_3$] ratio of 1:1 [14].

Table 2 Atomic positions for $CoCu_2O_3$ in fractional coordinate.

	x	*y*	*z*	site[1]	parameters[2]
Co	0.25	0.25	0.42	2a	*z* = 0.42
Co	0.75	0.75	0.58	2a	*z* = 0.42
Cu	0.08	0.75	0.85	4f	*x* = 0.08, *z* = 0.85
Cu	0.42	0.75	0.85	4f	*x* = 0.08, *z* = 0.85
Cu	0.58	0.25	0.15	4f	*x* = 0.08, *z* = 0.85
Cu	0.92	0.25	0.15	4f	*x* = 0.08, *z* = 0.85
O	0.12	0.25	0.95	4f	*x* = 0.12, *z* = 0.95
O	0.38	0.25	0.95	4f	*x* = 0.12, *z* = 0.95
O	0.62	0.75	0.05	4f	*x* = 0.12, *z* = 0.95
O	0.88	0.75	0.05	4f	*x* = 0.12, *z* = 0.95
O	0.25	0.75	0.50	2b	*z* = 0.50
O	0.75	0.25	0.50	2b	*z* = 0.50

[1]Site in the International Tables for Crystallography no. 59, p. 293.
[2]Obtained from VASP simulation.

Crystal structures of the identified phases were analyzed based on the space group information from the ICDD data, International Tables for Crystallography [15], and simulation using VASP code. Simulation methodology comprises plane-wave density functional theory (DFT), spin-polarized PAW-GGA functional [16], van der Waals correction by Grimme [17], and a Gaussian smearing. To ensure convergence results, all stages used plane wave cut off energy of 500 eV. Completion of iterations entailed tolerances of less than 0.1 meV for energy and less than 0.05 eV/Å for atomic forces. Lattice parameters from literature values (ICDD), our XRD experiment data and VASP simulations are tabulated in Tables 1-3. The $CoCu_2O_3$ is a type of spin ladder crystal [18, 19]. It is seen in Table 1, the lattice parameters from three sources (ICDD, our XRD and VASP) are in good agreement.

Table 3 Atomic positions for $CoCuO_2$ or $CuCoO_2$ in fractional coordinate

	x	*y*	*z*	site[1]	parameter[2]
Cu	0.00	0.00	0.00	1a	-
Co	0.50	0.50	0.50	1b	-
O	0.11	0.11	0.11	2c	*x* = 0.11
O	0.89	0.89	0.89	2c	*x* = 0.11

[1]Site in the International Tables for Crystallography no. 166, p. 547.
[2]Obtained from VASP simulation.

3.2. Surface electronic structure

The Cu *2p* XPS spectra of CoO/CuO films synthesized at different annealing temperatures are shown in Figure 2. All of the spectra show two main peaks of Cu $2p_{3/2}$ and Cu $2p_{1/2}$ and satellites on the high energy side of these two main peaks. The separation between the Cu $2p_{1/2}$ and Cu $2p_{3/2}$ peaks slightly increases as the temperature is increased from 500°C to 650°C. This subtle increase from 19.7 eV to 19.85 eV indicates the existence of a low oxidation state of copper, while the satellite peaks indicate the presence of Cu^{2+} and an open $3d^9$ shell [20].

Figure 3 shows the decoupling of Cu $2p_{3/2}$ peaks and the satellites at different annealing temperatures. Table 4 lists the binding energies and the percentages of the four components from the decouplings. Generally, the increase of annealing temperature does not change the Cu bonding structure significantly. The percentages for the tetrahedral Cu^+ ions and the octahedral Cu^{2+} ions are observed to be relatively equal (approx. 1:1 ratio) except for coating synthesized at 500°C which has a much higher percentage of

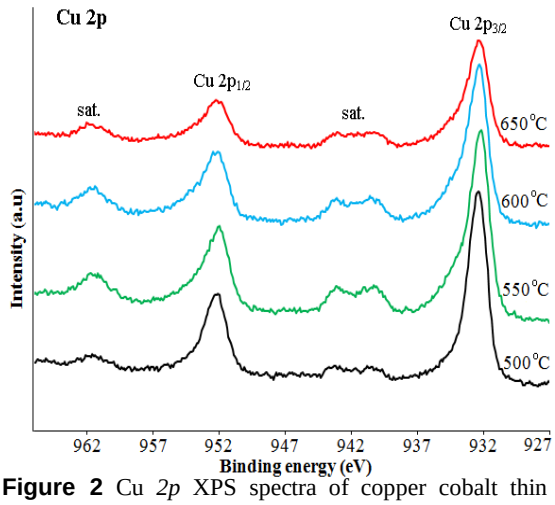

Figure 2 Cu *2p* XPS spectra of copper cobalt thin film coatings synthesized at different annealing temperatures

tetrahedral Cu^{+} (approx. 2:1 ratio). Increasing annealing temperature tends to decrease the number of tetrahedral Cu^{+} ions.

Figure 4, shows plots of the intensity ratios of Cu $2p_{3/2}$ satellite to Cu $2p_{3/2}$ main peak (I_{sat}/I_{main}) and the separation distance between the satellite and main peak. Overall the trend is an increase in the intensity ratio and a decrease in the separation distance as the annealing temperature varies from 500 °C to 650 °C. According to the Sawatzky theory [21], the shorter separation between the Cu $2p_{3/2}$ line and its satellite peak, and the higher I_{sat}/I_{main} ratio points to a decrease in the covalent character of the Cu-O bond in CoO/CuO coatings as compared to CuO [9].

The XPS profile of Co *2p* spectra of the CoO/CuO coatings are shown in Figure 5. All spectra have two main peaks, namely Co $2p_{3/2}$ and Co $2p_{1/2}$, with their satellites located on the high energy sides of the main peak. Even though the intensities ratio of Co $2p_{1/2}$ to Co $2p_{3/2}$ for all coatings are relatively similar, the separations between Co $2p_{3/2}$ and Co $2p_{1/2}$ peaks owing to the spin-orbit splitting are still different. The spin-orbit splittings for the samples annealed at 550 °C and 600 °C are ~16.1 eV, while that for samples annealed at 500°C and 650 °C are ~15.9 eV. However, this evidence could correspond to the Co^{2+} ions confirmed by the presence of characteristic satellites in between of Co $2p_{3/2}$ and Co$2p_{1/2}$.

Besides the presence of cobalt ions in a partial spinel-type lattice arrangement, the relatively low intensities of satellites detected at 786 eV also indicate the presence of Co^{2+} ions mixed with Co^{3+} ions [5]. The existence of this ions mixing is confirmed by the asymmetry of Co $2p_{1/2}$ peaks [14].

Figures 6.a-d show the decoupling of the Co $2p_{3/2}$ peaks and their satellites resulting in five curve-fitted components. The peaks at around 780 eV (denoted "ii") are mostly due to the mixed Co(II,III) bonding states whereas the component with binding energy lower than 780 eV (denoted "i") are predominantly attributed to Co^{3+} in

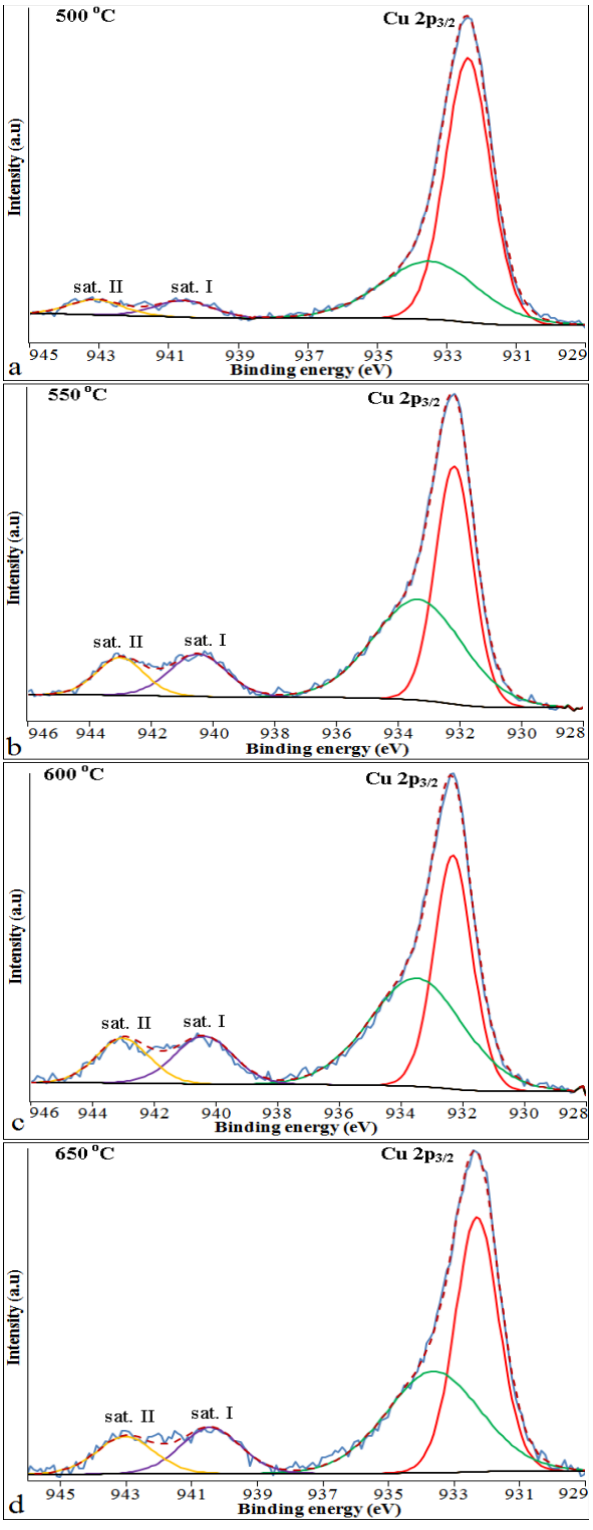

Figure 3 Decoupling of Cu $2p_{3/2}$ peaks of copper cobalt thin film coatings synthesized at different annealing temperatures.

octahedral coordination and the components with binding energy of Co $2p_{3/2}$ greater than 780 eV with a shake-up satellite are the characteristics of Co^{2+} in tetrahedral coordination. Table 5 represents the details of binding energy

Table 4 The curve-fittings results of Cu $2p_{3/2}$ and its satellites of copper cobalt films synthesized at different annealing temperatures

Annealing temperature	Binding energy and percentage			
	Cu $2p_{3/2}$ photoelectron line		Satellite I	Satellite II
500 °C	932.4 eV (61.7 %)	933.5 eV (29.05 %)	940.6 eV (5.0 %)	943.1 eV (4.3 %)
550 °C	932.2 eV (40.3 %)	933.35 eV (40.7 %)	940.5 eV (10.9 %)	943.0 eV (8.1 %)
600 °C	932.3 eV (36.9 %)	933.5 eV (41.8 %)	940.4 eV (11.5 %)	943.0 eV (9.7 %)
650 °C	932.3 eV (43.45%)	933.6 eV (37.3 %)	940.4 eV (10.8 %)	943.0 eV (8.4 %)
Attributions:	Tetrahedral Cu^{+}	Octahedral Cu^{2+}	Cu^{2+} characteristic satellites	

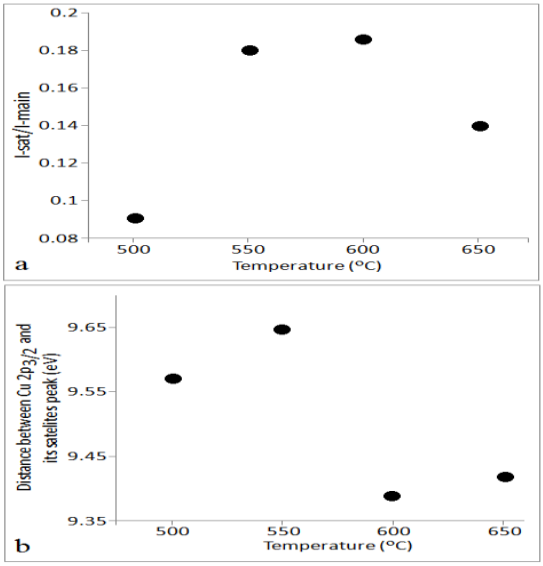

Figure 4 Cu $2p_{3/2}$ satellite intensity to Cu $2p_{3/2}$ main peak intensity ratio (I_{sat}/I_{main}) values with the increase of annealing temperature (a), and the distances between the Cu $2p_{3/2}$ line and its satellites peak with the increase of annealing temperature from 500 °C to 650 °C.

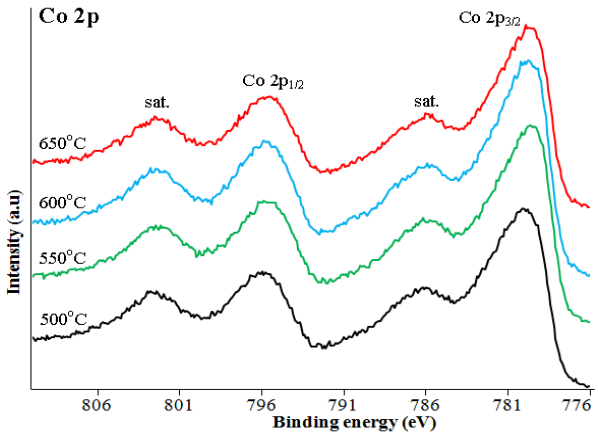

Figure 5 Co *2p* XPS spectra of copper cobalt thin film coatings synthesized at different annealing temperatures.

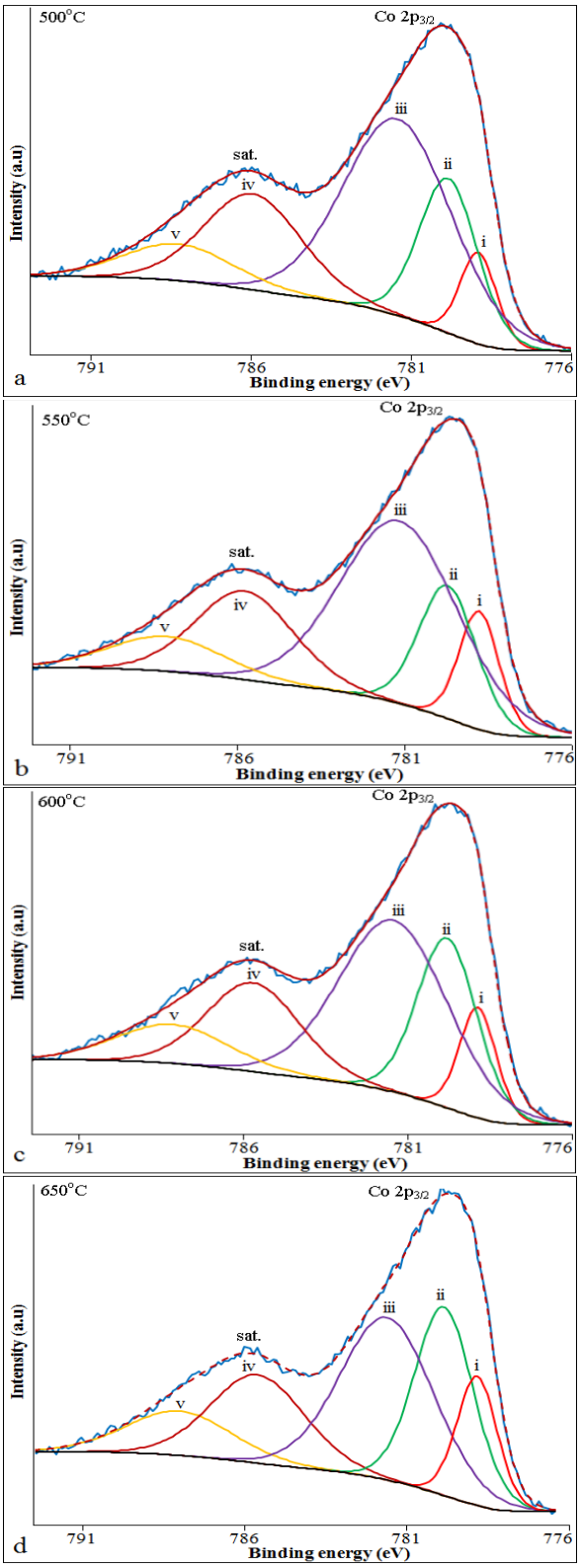

Figure 6 Decoupling of Co $2p_{3/2}$ peaks and their sattelites of copper cobalt thin film coatings synthesized at different annealing temperatures.

Table 5 Binding energies and percentages of decoupling results of Co $2p_{3/2}$ peaks

Anne-aling	Binding energy and percentage				
	Co $2p_{3/2}$ photoelectron line			satellites	
	i	ii	iii	iv	v
500 °C	778.9 eV (7.1 %)	779.9 eV (19.1 %)	781.4 eV (45.4 %)	786.0 eV (19.85 %)	788.3 eV (8.6 %)
550 °C	778.8 eV (10.2 %)	779.7 eV (16.4 %)	781.2 eV (46.3 %)	785.8 eV (18.6 %)	788.1 eV (8.6 %)
600 °C	778.9 eV (9.0 %)	779.8 eV (22.3 %)	781.4 eV (41.0 %)	785.7 eV (18.1 %)	788.2 eV (9.6 %)
650 °C	778.8 eV (11.7 %)	779.8 eV (25.0 %)	781.6 eV (34.2 %)	785.6 eV (18.6 %)	788.0 eV (10.5 %)
Attri-butions	Octa-hedral Co(III)	Co(II,III)	Tetra-hedral Co(II)	Co(II) characteristic satellites	

and the percentages of each component. It is also seen in all the samples, the tetrahedral Co^{2+} ions are prominent, and the increase in temperature tends to decrease the number of Co^{2+} ions. In the case of CoO/CuO system, the Co^{2+} ions are partially substituted by Cu^{2+} ions [1, 10] forming copper–cobalt oxide structures [5].

The curve fitted O *1s* XPS spectra of CoO/CuO film coatings are presented in Figure 7a-d. Generally, there is relatively no change in the oxygen surface compositions when the coatings were treated at different annealing temperatures from 500 °C to 650 °C. In each sample, the spectrum shows a strong peak around 529.3 eV with an apparent shoulder at the higher binding energy side (denoted X).

The four components are results from decoupling of each photoelectron spectrum. The components at binding energy (BE) of around 529.2-529.5 eV (denoted "i") are due to lattice O^{2-} in the structure whereas at BE of around 530.4-531.4 eV (denoted "ii" and "iii") may be attributed to the surface oxygen from a wide variety of species (chemisorbed oxygen O^-, oxygen containing surface contamination, and/or OH-like species, as hydroxyl, carbonate groups, *etc.*) [1, 5, 9, 22-25]. The sub-surface O^- specieses are also observed at BE around 532.1-532.4 eV (denoted "iv") [26, 27]. The features exhibited by the shoulders at the high energy side of the O *1s* main peaks are the characteristics of the copper-cobalt mixed oxides family which distinguish them from O *1s* of Co_3O_4 in single component [1].

3.3. Optical properties The absorptance (α) value is the basic characterization of the optical properties of CoO/CuO coatings on Al substrate (absorber-reflector tandem system). It can be measured in terms of reflectance as described by Duffie and Beckman [13]. High spectral reflectance indicates low absorptance and *vice versa*. Figure 8 shows the reflectance spectra and the corresponding solar absorptance values of coatings on highly reflective aluminium substrates synthesized at different annealing temperatures.

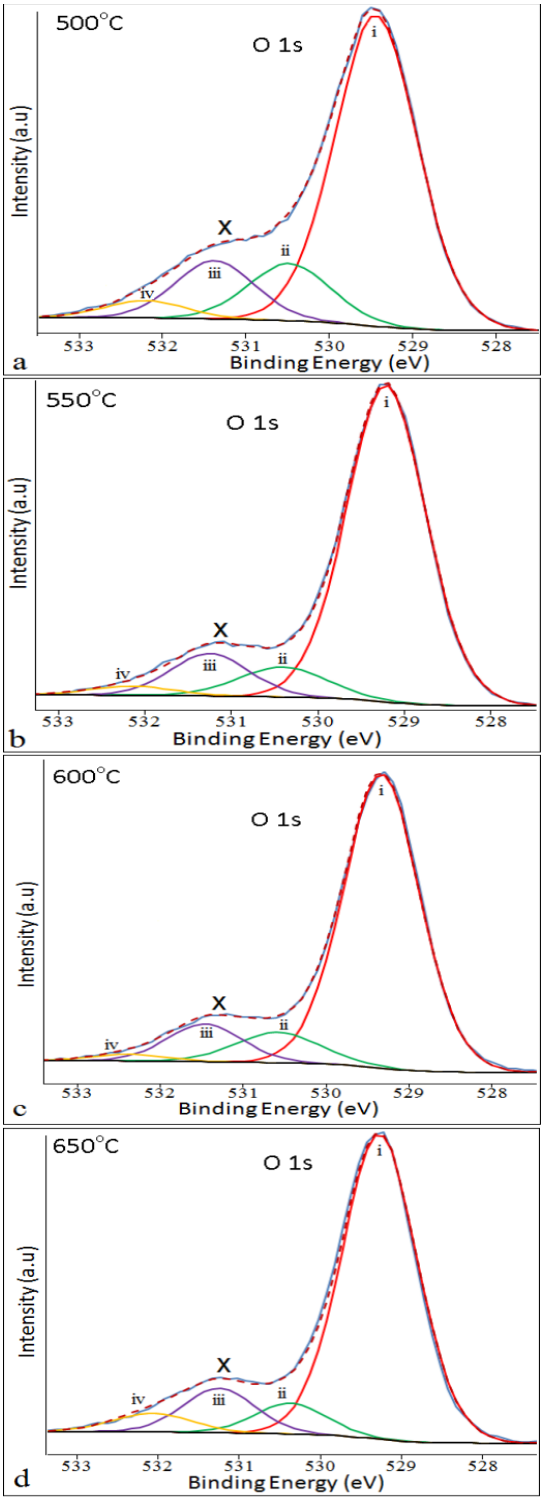

Figure 7 O *1s* XPS spectra and curve-fittings of copper cobalt thin film coatings synthesized at different annealing temperatures.

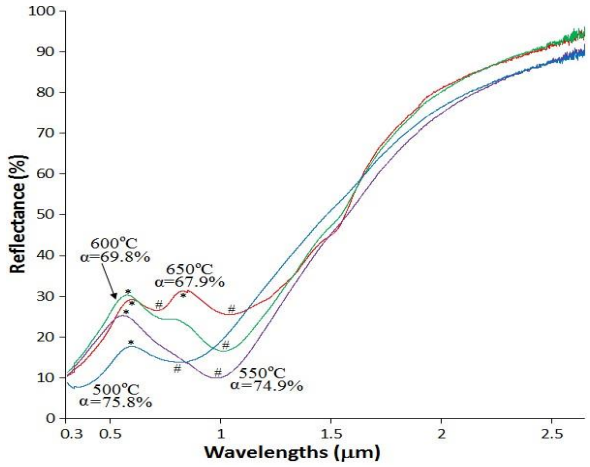

Figure 8 Reflectance spectra with solar absorptance of copper–cobalt oxide thin film coatings on reflective aluminium substrates synthesized at different annealing temperatures.

Generally, the coatings exhibit low reflectance with 1 or 2 minor maxima below 1.5 μm and moderate to high reflectance above 1.5 μm which form the basis of a solar selective absorber profile. In the absorber-reflector tandem system, low reflectance spectra at lower wavelengths are attributed to the interactions between the incoming solar radiation and the coating material. In this area, most of the incoming solar radiation will be absorbed by the coating surface. There are maxima/minima in the low wavelengths area consisting of the interference peaks (labelled "*") and the absorption edges (labelled "#") below 1.2 μm. For coatings synthesized at 650 °C, it is apparent that more than one interference peak and one absorption edge were found. This may associated with the change of oxide phases ratio as elucidated in the previous structural section (Section 3.1.).

In terms of temperature change, the interference peaks and the absorption edges positions tend to raise with the increase of annealing temperature that eventually lowers the solar absorptance up to 10%. Figure 9 is a plot of Absorptance vs Temperature and clearly shows a decrease in absorptance as temperature increases. This indicates that the higher the heating temperature, the smaller the ability of coating material to absorpt the UV-Vis light with little influence on NIR light. The phenomena in this temperature range can be utilized for absorptance tuning without much change in the NIR absorption. The moderate to high reflectance spectra seen above 1.5 μm are mainly attributed to the interactions between the transmittant incoming infrared radiation and the reflective aluminum surface. Basically, for coatings with similar thicknesses, the reflectance profiles above 1.5 μm featured in Figure 8 are due to the resultant transmitted infrared beam *via* coating material (akin to semiconductor properties) and its reflection back by the substrate surface.

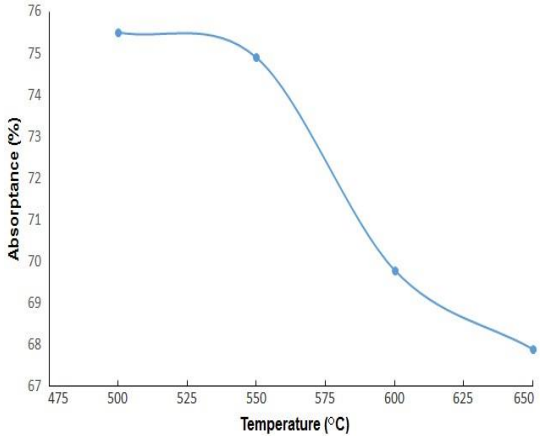

Figure 9 The absorptance versus the annealing temperatures

3.4. Nanoindentation tests Figure 10 shows the elastic modulus (*E*), hardness (*H*) and *H/E* of the coatings caharacterized via nanoindentation tests. There is a desired impact on the mechanical properties of the coating layer where both the elastic modulus and the hardness increase with increasing annealing temperature, especially for coatings synthesized above 550°C. Both the elastic modulus and the hardness of these coatings were increased up to 20% above 550 °C. The associated errors in both the modulus and hardness data are attributed to the porosity and the surface roughness factors of the coatings [4, 12, 14].

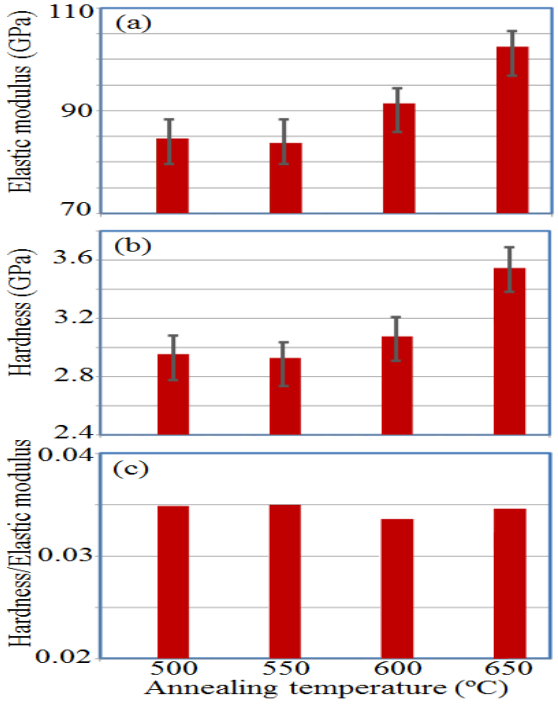

Figure 10 Mechanical properties of the deposited coatings obtained from the nanoindentation tests, (a) elastic modulus, (b) hardness, and (c) *H/E*.

The parameter *H/E* is used to predict the wear resistance of the thin film coatings [28]. The wear resistance is an important factor in the performance and function of the optical coatings during their operations where mechanical contacts are always expected [29]. No significant changes in *H/E* were found after the heat treatment of the coatings. The wear resistance values tend to be stable at 0.035. It is a surprise getting stable wear resistance of coatings synthesized using a low sol precursor concentration (Figure 10c) due to the increase in the hardness, as the increase of temperature is followed by an increase of elastic modulus proportionally. It is different from our previous report [14] where the critical point of the overall wear resistance deflation was at temperature of 650ºC. If it is linked to the structural analysis, it is clear that the enhancement of $[CoCuO_2/CuCoO_2]:[CoCu_2O_3]$ oxide phases ratio indicated at annealing temperature of 650ºC in this report has a direct impact to retain the wear resistance from degradations. Table 6 describes the qualitative differences of structural and mechanical properties of between the present and the previous work [14] for annealing temperature of 650 °C. Overall, coatings prepared in this work are envisaged to have superior wear resistance compared to the aluminum substrate (*H/E*=0.011) [4, 14].

Table VI Qualitative differences between present and previous work for the 650 °C annealing temperature

Properties	Previous report [14]	Present
$[CoCuO_2/CuCoO_2]:[CoCu_2O_3]$	1:1	3:2
Elastic Modulus	Linear trend	Non-linear trend
Hardness	constant	Non-linear trend
H/E	Decreasing trend	constant

Conclusions

Cobalt and copper mixed oxides thin films have been coated on aluminum substrate via sol-gel route using low concentration of copper and cobalt sol precursors (thereby enhancing cost-effectiveness of the coatings). The coatings exhibited a low crystallinity of $CoCu_2O_3$, $CoCuO_2$ and $CuCoO_2$. The surface bonding structure analysis indicated that the surface contained tetrahedral Cu^+ and octahedral Cu^{2+}, octahedral Co^{3+}, tetrahedral Co^{2+} and mixed Co^{2+} and Co^{3+}, as well as lattice, surface and sub-surcafe oxygens. The observed optical properties exhibited distinctive spectral selectivity in the solar wavelengths region (<2.5 μm). Throughout this study we found that coatings synthesized at low concentration of sol precursors exhibited a favourable stable wear resistance (*H/E*) at high operating temperatures due to the change of the $[CoCuO_2/CuCoO_2]:[CoCu_2O_3]$ oxide phases ratio as the annealing temperature was increased.

Acknowledgements We would like to acknowledge Indonesia Government for the research funding under the "Kerjasama Luar Negeri & Publikasi Internasional" research scheme (Grant No. 548/UN. 19.5.1.3/LT/2015). Many thanks to Mr John Boulton and Mr Ken Seymour for their assistance in the analyses. Z.T. Jiang is grateful for the small grant scheme 2014, School of Engineering and Information Technology, Murdoch University. C.Y. Yin is supported by the Teesside University Research Fund (URF).

References

[1] M. De Koninck, S.C. Poirier, B. Marsan, J. Electrochem. Soc. 153, A2103 (2006)
[2] D. J. Singh, Phy. Rev. B 76, 85110 (2007)
[3] M. Beekman, J. Salvador, X. Shi, G. S. Nolas, J. Yang, J. Alloy Compd. 489, 336 (2010)
[4] A. Amri, Z.-T. Jiang, T. Pryor, C.-Y. Yin, Z. Xie, N. Mondinos, Surf. Coat. Tech. 207, 367 (2012)
[5] J. L. Gautier, E. Trollund, E. Ríos, P. Nkeng, G. Poillerat, J. Electroanal. Chem. 428, 47 (1997)
[6] R. N. Singh, J. P. Pandey, N. K. Singh, B. Lal, P. Chartier, J. F. Koenig, Electrochim. Acta 45, 1911 (2000)
[7] A. Amri, ZT. Jiang, N. Wyatt, CY. Yin, N. Mondinos, T. Pryor, M.M. Rahman, Ceram. Intl. 40, 16569 (2014).
[8] W. M. Shaheen, A. A. Ali, Mater. Res. Bull. 36, 1703 (2001)
[9] A. La Rosa-Toro, R. Berenguer, C. Quijada, F. Montilla, E. Morallon, J. L. Vazquez, J. Phys. Chem. B 110, 24021 (2006)
[10] G. Fierro, M. Lo Jacono, M. Inversi, R. Dragone, P. Porta, Top. Catal. 10, 39 (2000)
[11] A. Amri, Z.-T. Jiang, P.A. Bahri, C.-Y. Yin, X. Zhao, Z. Xie, X. Duan, H. Widjaja, M.M. Rahman, T. Pryor, J.Phys. Chem. C, 117, 16457 (2013).
[12] A. Amri, X. Duan, C.-Y. Yin, Z.-T. Jiang, M.M. Rahman, T. Pryor, Appl. Surf. Sci. 275, 127 (2013)
[13] J.A. Duffie, W.A. Beckman, Solar Engineering of Thermal Processes, third ed., (John Wiley & Sons Inc., New Jersey, 2006)
[14] A. Amri, Z.-T. Jiang, X. Zhao, Z. Xie, C.-Y. Yin, N. Ali, N. Mondinos, M.M. Rahman, D. Habibi, Surf. Coat. Tech. 239, 212 (2014).
[15] E. Theo Hahn, International Tables for Crystallography Volume A: Space-Group Symmetry, 5th ed. (Springer 2005).
[16] J.P. Perdew, K. Burke, Y. Wang, Phys. Rev. B 54, 16533 (1996).
[17] S. Grimme, J. Compu. Chem. 27, 1787 (2006).
[18] K. Oh-ishi, Y. Tsuchiya, Y. Iizuka, H. Yamane, J. Solid State Chem. 160, 251 (2001)
[19] E. Bordas, C.d. Graaf, R. Caballol, C.J. Calzado, Phys. Rev. B 71, 45108 (2005)

[20] M. Brandhorst, J. Zajac, D.J. Jones, J. Rozière, M. Womes, A. Jimenez-López, E. Rodríguez-Castellón, Appl. Catal. B 55, 267 (2005)
[21] D.K.G. de Boer, C. Haas, G.A. Sawatzky, Phys. Rev. B 29, 4401 (1984)
[22] T.J. Chuang, C.R. Brundle, D.W. Rice, Surf. Sci. 59, 413 (1976)
[23] G. Tyuliev, D. Panayotov, I. Avramova, D. Stoichev, T. Marinova, Mat. Sci. Eng. C 23, 117 (2003)
[24] P. Stefanov, I. Avramova, D. Stoichev, N. Radic, B. Grbic, T. Marinova, Appl. Surf. Sci. 245, 65 (2005)
[25] G. Tyuliev, S. Angelov, Appl. Surf. Sci., 32, 381 (1988)
[26] J.-C. Dupin, D. Gonbeau, P. Vinatier, A. Levasseur, Phys. Chem. Chem. Phys. 2, 1319 (2000)
[27] S. Royer, A. Van Neste, R. Davidson, S. Mcintyre, S. Kaliaguine, Ind. Eng.Chem. Res. 43, 5670 (2004)
[28] A. Leyland, A. Matthews, Wear 246, 1 (2000)
[29] J.G. Meier, A. Mrzel, M. Canales, P. Gonzalvo, N. Alcala, Phys. Status Solidi A 210, 2307 (2013)